DAEHAN HWAHAK HWOEJEE
(*Journal of the Korean Chemical Society*)
Vol. 26, No. 3, 1982
Printed in the Republic of Korea

유기분자의 내부 회전장벽에 관한 이론적 연구 (제 1 보). 에탄에서의 중심 탄소의 역할

金英植 · 金鎬澈†
서울대학교 자연과학대학 화학과

(1981. 12. 31 접수)

On the Rotational Barrier of Organic Molecules (I). Role of Axial Carbon in Ethane

Young Sik Kim and **Hojing Kim**†
Department of Chemistry, College of Natural Sciences
Seoul National University, Seoul 151, Korea

(Received Dec. 31, 1981)

요 약. 에탄의 회전 장벽에 미치는 두개의 탄소 원자의 영향을 알아보기 위해 6개의 수소만으로 이루어진 탄소가 없는 에탄을 모델로 택하여 이 모델 분자의 Staggered 및 eclipsed 꼴의 에너지를 Mcweeny 의 open-shell RHF-SCF 방법으로 계산하고, staggered 에서 eclipsed 로 꼴이 변할때의 천이밀도를 조사 하였다. 예상대로 모델 분자에서는 ecliped 꼴이 staggered 꼴보다 안정하였다. 이 탄소없는 에탄의 천이 밀도와 실제 에탄의 천이 밀도를 비교 분석하여, 에탄의 회전 장벽은 중심축 위치에 있는 두개의 탄소 원자로 인해 staggered 에서 eclipsed 꼴로 변함에 따라 수소 원자 주위의 전자 밀도가 희석되고, 탄소 원자 주위와 탄소-탄소 결합 공간으로 끌리므로 해서, 전자 에너지 감소가 핵간 반발 에너지의 증가를 상쇄하지 못하는데 기인한다는 것을 알게 되었다.

ABSTRACT. In order to analyze the role of axial carbon atoms in rotational barrier of ethane, we take the carbonless ethane, as a model, which is made of six hydrogens in coordinates of ethane. The energy of the system is calculated by McWeeny's open-shell restricted Hartree-Fock selfconsistent-field (RHF-SCF) method, and the transition density on the staggered-to-eclipsed rotation is examined. As being expected, the eclipsed form of the model is more stable than the staggered one. Through the transition density comparison of this model and real ethane, it is found that the existence of the axial carbon atoms induces the electronic density to be diluted in the vicinity of protonic sites and to be attracted to the region of carbon atoms or further to C-C bond region as the barrier is traversed. This migration of electronic charge tell us that the barrier to the internal rotation of ethane originates from the fact that the magnitude of electronic energy depression is not large enough to offset the increased nuclear-nuclear repulsion on the staggered-to-eclipsed rotation.

1. INTRODUCTION

When a molecule experiences a deformation of the nuclear skeleton from a less-crowded conformation to a more-crowded one, nuclear-nuclear repulsion plus the electronic energy (in the framework of non-relativistic Born-Oppenheimer approximation) may increase or decrease

depending on the negating effect of the electronic energy depression on the increased nuclear-nuclear repulsion. In the case of ethane, a typical organic molecule with internal rotation, the magnitude of electronic energy depression is not large enough to offset the increased nuclear-nuclear repulsion on staggered-to-eclipsed conformational change. The electronic energy change is, of course, originated from an alternation of the electronic environment around and between atomic nuclei of the molecule. A closer observation shows that a part of the electronic rearrangement contributes to elevation of the energy and another part of the rearrangement has the effect of energy depression, although the net effect is the depression. In terms of "origin of barrier", what we really mean is the origin of electronic portion of the barrier, that is, a close profile of the portion of electronic rearrangement having energy-enhancing effect. In the previous work,[1] it is found, through the transition density analysis, that the electronic portion of the barrier of ethane is originated from the migration of the electronic charge from the general vicinity of the moving hydrogen nuclei to carbon located on the rotational axis as the barrier is traversed.

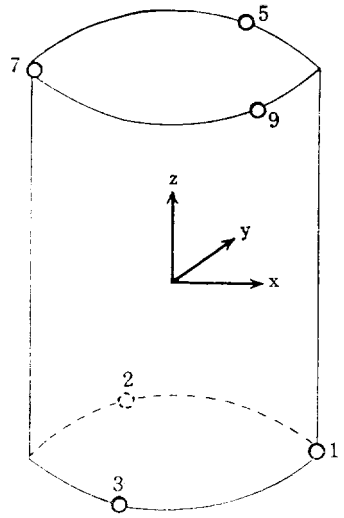

Fig. 1-1. The position of hydrogens in staggered conformation.

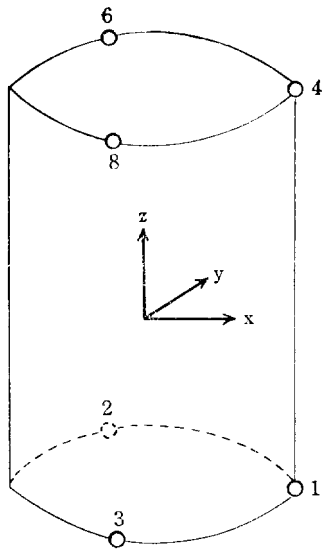

Fig. 1-2. The position of hydrogens in eclipsed conformation.

The objective of the present work is to justify the previous claim[1] (the role of carbon atoms on the barrier), by showing the disappearance of the electronic portion of barrier by extracting carbon atoms away.

We take carbonless ethane, the imaginary molecule of 6 hydrogens in the geometry of ethane, as the model (see *Fig.* 1). The restricted Hartree-Fock selfconsistent-field formalism is employed for the energy calculation of each conformation. We use the coordinates of Pizer and Lipscomb,[2] and geometry optimization is dismissed. The transition density analysis is carried out in order to see explicitly the role of axial carbon to the barrier.

2. McWEENY'S OPEN-SHELL RESTRICTED HARTREE-FOCK SCFFORMALISM[3~5]

The space groups of staggered-and eclipsed-

carbonless ethane conformations are D_{3d} and D_{3h}, respectively.

The configurations of these are $(a_{1g})^2(a_{2u})^2(e_u)^2$ and $(a_1')^2(a_2'')^2(e')^2$ respectively.

According to Hund's rule, each lowest energy state of these configuration is $^3\Sigma^-$. Let's make use of McWeeny's open-shell RHF-SCF formalism in order to determine the optimum MO's for each state.

The energy expression is

$$E=\nu_1[\sum_A\langle A|h|A\rangle+\frac{1}{2}\nu_1\sum_{A,B}(\langle AB|g|AB\rangle-\frac{1}{2}\langle AB|g|BA\rangle)]+\nu_2[\sum_U\langle U|h|U\rangle+\frac{1}{2}\nu_2\sum_{U,V}(\langle UV|g|UV\rangle-\langle UV|g|VU\rangle)]+\nu_1\nu_2[\sum_{A,U}(\langle AU|g|AU\rangle-\frac{1}{2}\langle AU|g|UA\rangle)] \quad (1)$$

where $A, B, \ldots\ldots$: Closed shell orbitals ;
$U, V, \ldots\ldots$: Open shell orbitals ;
ν_1 : Closed shell occupation number ;
ν_2 : Open shell occupation number.

According to Roothaan's LCAO-MO SCF method, the molecular orbitals $A, B, \ldots\ldots, U, V, \ldots$ ...can be expressed as a linear combination of basis functions $\{\phi_k\}$ which is initially assumed orthonormal.

$$(ABC\cdots)=(\phi_1\phi_2\ldots)\boldsymbol{T}_1 \quad (2)$$
$$(UV\ldots\ldots)=(\phi_1\phi_2\cdots)\boldsymbol{T}_2 \quad (3)$$

where
$$\boldsymbol{T}_1=(\boldsymbol{C}_A|\boldsymbol{C}_B|\cdots) \quad (4)$$
$$\boldsymbol{T}_2=(\boldsymbol{C}_U|\boldsymbol{C}_V|\cdots) \quad (5)$$

and the column vectors $\boldsymbol{C}_A, \boldsymbol{C}_B, \cdots$or $\boldsymbol{C}_U, \boldsymbol{C}_V, \cdots$ are the expansion coefficients of $A, B, \cdots$or $U, V, \cdots$respectively. And we define density matrices for each shell

$$\boldsymbol{R}_1=\boldsymbol{T}_1\boldsymbol{T}_1^+ \qquad \boldsymbol{R}_2=\boldsymbol{T}_2\boldsymbol{T}_2^+ \quad (6)$$

The orthonormality conditions may be replaced by equivalent condition on the density matrices defined by eq. (6).
Thus

$$\boldsymbol{R}_1^2=\boldsymbol{R}_1, \quad \boldsymbol{R}_2^2=\boldsymbol{R}_2, \quad \boldsymbol{R}_1\boldsymbol{R}_2=\boldsymbol{0} \quad (7)$$

where the third expression describes the orthogonality condition of the closed-and open-shell MO's.
From eqs. (1) and (6), we obtain

$$E=\nu_1 tr\boldsymbol{R}_1(\boldsymbol{h}+\frac{1}{2}\boldsymbol{G}_1)+\nu_2 tr\boldsymbol{R}_2(\boldsymbol{h}+\frac{1}{2}\boldsymbol{G}_2) \quad (8)$$

where electron interaction matrices $\boldsymbol{G}_1, \boldsymbol{G}_2$ of the two shells, which are slightly different, are given by

$$\boldsymbol{G}_1=\boldsymbol{G}(\nu_1\boldsymbol{R}_1)+\boldsymbol{G}(\nu_2\boldsymbol{R}_2) \text{ (closed shell)} \quad (9)$$
$$\boldsymbol{G}_2=\boldsymbol{G}(\nu_1\boldsymbol{R}_1)+\boldsymbol{G}'(\nu_2\boldsymbol{R}_2) \text{ (open shell)} \quad (10)$$

where G and G', expressed in terms of coulomb and exchange matrices,
are

$$\boldsymbol{G}(\boldsymbol{R})=\boldsymbol{J}(\boldsymbol{R})-\frac{1}{2}\boldsymbol{K}(\boldsymbol{R}) \quad (11)$$
$$\boldsymbol{G}'(\boldsymbol{R})=\boldsymbol{J}(\boldsymbol{R})-\boldsymbol{K}(\boldsymbol{R}) \quad (12)$$

and the matrix elements of the one-electron Hamiltonian h, J and K are given by [6~12]

$$\boldsymbol{h}_{ij}=\langle\phi_i|h|\phi_j\rangle \quad (13)$$
$$\boldsymbol{J}(\boldsymbol{R})_{ij}=\sum_{k,l}R_{lk}\langle\phi_i\phi_k|g|\phi_j\phi_l\rangle \quad (14)$$
$$\boldsymbol{K}(\boldsymbol{R})_{ij}=\sum_{k,l}R_{lk}\langle\phi_i\phi_k|g|\phi_l\phi_j\rangle \quad (15)$$

By the variation method constrained to the orthonormality condition eq. (7), we can derive the orbital energy expression

$$\bar{h}\boldsymbol{C}=\epsilon\boldsymbol{C} \quad (16)$$

in which the effective Hamiltonian[4] is

$$\bar{h}=\boldsymbol{R}_2'\boldsymbol{h}_1\boldsymbol{R}_2'+\boldsymbol{R}_3'\boldsymbol{h}_2\boldsymbol{R}_3'+\boldsymbol{R}_3'(2\boldsymbol{h}_1-\boldsymbol{h}_2)\boldsymbol{R}_3' \quad (17)$$

where $\boldsymbol{R}_i'=\boldsymbol{1}-\boldsymbol{R}_i$ is defined as the projector complementary to R_i and each projection operators $\boldsymbol{R}_1, \boldsymbol{R}_2$ and $\boldsymbol{R}_3$ $(=\boldsymbol{1}-\boldsymbol{R}_1-\boldsymbol{R}_2)$ corresponds to the doubly, singly occupied and empty MO's.
If the basis set $\{\phi_k\}$ is not orthonormal, then eq. (16) is replaced by

$$\hbar C=\epsilon SC \tag{18}$$

The constraints eq. (7) become, in the non-orthogonal case,

$$R_1SR_1=R_1,\ R_2SR_2=R_2,\ R_1SR_2=O \tag{19}$$

Let's transform the non-orthogonal set $\{\phi_k\}$ into an orthogonal set $\{x\}$ and, correspondingly, $\hbar^\phi$ into $\hbar^x$.[13]

Now $\hbar^x$ can be diagonalized by an orthogonal transformation, and this will permit the calculation of the coefficient matrix C.

$$\phi=\phi C=\phi VU=xU \tag{20}$$

Substituting eq. (20) into eq. (18), we have

$$C^+\hbar^\phi C=C^+S^\phi C\epsilon \tag{21}$$

$$U^+\underbrace{V^+\hbar^\phi V}_{\hbar^x}U=U^+\underbrace{V^+S^\phi V}_{S^x=1}U\epsilon \tag{22}$$

and then

$$U^+\hbar^xU=U^+U\epsilon=\epsilon \tag{23}$$

where ϵ is a diagonal matrix.

Lõwdin showed that the unitary matrix V may be chosen to be $S^{-1/2}$, *i.e.* $V=S^{-1/2}$. With this choice, one has Lõwdin orthogonalization:

1st step: Diagonalization $\theta^+S\theta=D$
where θ is orthogonal matrix

2nd step: Rasing D to the $-1/2$ power
$D^{-1/2}$

3rd step: Backtransformation
$S^{-1/2}=\theta D^{-1/2}\theta^+$

where the process from 2nd to 3rd step is based on the special properties of diagonal matrices, according to which any operation on the diagonal element is equivalent to the same operation on the whole matrix. Thus, if $V=S^{-1/2}$, then $V^+SV=1$[12,13]

3. TRANSITION DENSITY AND CORRESPONDING ORBITALS

Rotational barrier for the change of x to y conformation is given by the IHF theorem[15] as follows

$$\begin{aligned}\Delta E^{IHF}&=\langle\Phi_x|H_y-H_x|\Phi_y\rangle\langle\Phi_x|\Phi_y\rangle^{-1}\\&=\Delta E_{NN}+\Delta E_{el}{}^{IHF}\\&=\Delta E_{NN}+\int\Delta v(1)\rho_{xy}(1)d\tau_1\end{aligned} \tag{24}$$

where $\Delta v(1)$ is the difference of the nuclear-electron attraction potentials of the two conformations, ΔE_{NN} is the difference of the nuclear-nuclear repulsion potentials, and $\rho_{xy}(1)$ is the transition density defined by

$$\rho_{xy}(1)=N\int\Phi_x{}^*\Phi_y d\tau_2d\tau_3\cdots d\tau_N/\int\Phi_x{}^*\Phi_x d\tau_1\cdots d\tau_N \tag{25}$$

(N; the number of electrons)

In the case of the carbonless ethane, the wave functions Φ_e, Φ_s for the eclipsed (e) and staggered (s) conformations are given by

$$\Phi_e=(6!)^{-1/2}\det\{a_1',\bar{a}_1',a_2'',\bar{a}_2'',e_x',e_y'\} \tag{26}$$

$$\Phi_s=(6!)^{-1/2}\det\{a_{1g},\bar{a}_{1g},a_{2u},\bar{a}_{2u},e_{ux},e_{uy}\} \tag{27}$$

where $a_1',a_2''\cdots$and $a_{1g},a_{2u}\cdots$, which are obtained by McWeeny's open-shell RHF-SCF method, are listed in *Table* 1 and *Table* 2.

And the transition density is shown by

$$\begin{aligned}\rho_{se}(1)&=6\int\Phi_s{}^*\Phi_e d\tau_2\cdots d\tau_6/\int\Phi_s{}^*\Phi_s d\tau_1\cdots d\tau_6\\&=\phi(1)\boldsymbol{d}^{-1}\phi^+(1)\end{aligned} \tag{28}$$

where $\phi=(a_1',\bar{a}_1',a_2'',\bar{a}_2'',e_x',e_y')$ and $\phi=(a_{1g},\bar{a}_{1g},a_{2u},\bar{a}_{2u},e_{ux},e_{uy})$ and $\boldsymbol{d}^{-1}$ is the inverse of the overlap matrix $\boldsymbol{d}=\{\langle\phi_i|\phi_j\rangle\}$

The overlap matrix $\boldsymbol{d}$ is given in *Table* 3 (for simplicity we consider overlaps between spin up wave functions).

The above matrix $\boldsymbol{d}$ is not diagonalized, but if we use the corresponding orbitals which are listed in *Table* 5, 6 the overlap matrix $\boldsymbol{D}$ between the corresponding orbitals, f_k and g_k, is diagonalized (see *Table* 4). Then the $\rho_{se}(1)$ is given simply by

$$\rho_{se}(1)=\sum_{k=1}^{4}\nu_kg_k(1)f_k{}^*(1)\langle f_k|g_k\rangle^{-1} \tag{29}$$

where $\nu_1=\nu_2=2$, $\nu_3=\nu_4=1$.

Eq. 29 tells us the corresponding orbitals are useful to trace the change of the real charge density and to analyze the contribution of each molecular orbital to the barrier.[1]

If we use the cylindrical coordinates (x axis is taken as $\phi=0$, see *Fig.* 1), then we define the effective transition density as

$$\begin{cases}\rho_{se}(r,\phi,z)-\rho_{se}(r,-\phi+\pi/3,z) \\ \qquad\qquad ;\ \phi\epsilon \text{ stabilizing region} \\ 0 \qquad\quad ;\ \phi\epsilon \text{ destabilizing region}\end{cases}$$

if $\rho_{se}(r,\phi,z)-\rho_{se}(r,-\phi+\pi/3,z)\geq 0$ at $\phi=0$.

$$\begin{cases}0 \qquad\quad ;\ \phi\epsilon \text{ stabilizing region} \\ \rho_{se}(r,\phi,z)-\rho_{se}(r,-\phi+\pi/3,z) \\ \qquad\qquad ;\ \phi\epsilon \text{ destabilizing region}\end{cases}$$

if $\rho_{se}(r,\phi,z)-\rho_{se}(r,-\phi+\pi/3,z)<0$ at $\phi=0$.

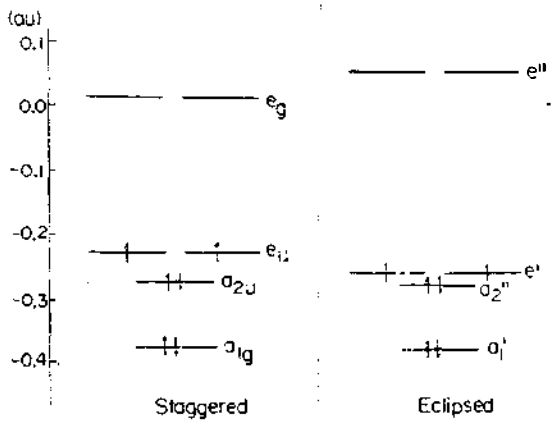

Fig. 2. MO energy level for carbonless-ethane.

Table 1. Occupied SCF-MO of eclipsed carbonless-ethane.

	a_1'	a_2''	e_x'	e_y'
1H-1s	0.300790	−0.363523	0.641475	0.0
2H-1s	0.300790	−0.363523	−0.320738	−0.555534
3H-1s	0.300790	−0.363523	−0.320738	0.555534
4H-1s	0.300790	0.363523	0.641475	0.0
6H-1s	0.300790	0.363523	−0.320738	−0.555534
8H-1s	0.300790	0.363523	−0.320738	0.555534

Table 2. Occupied SCF-MO of staggered carbonless-ethane.

	a_{1g}	a_{2u}	e_{ux}	e_{uy}
1H-1s	0.301267	−0.362687	0.651001	0.0
2H-1s	0.301267	−0.362687	−0.325500	−0.563783
3H-1s	0.301267	−0.362687	−0.325500	0.563783
5H-1s	0.301267	0.362687	0.325500	−0.563783
7H-1s	0.301267	0.362687	−0.651001	0.0
9H-1s	0.301267	0.362687	0.325500	0.563783

Table 3. Overlap integrals between eclipsed and staggered-carbonless-ethane.

	a_{1g}	a_{2u}	e_{ux}	e_{uy}
a_1'	0.956760	−0.050346	0.0	0.0
a_2''	−0.053985	0.937063	0.0	0.0
e_x'	0.0	0.0	0.795833	0.0
e_y'	0.0	0.0	0.0	0.795854

Table 4. Overlap integrals between the corresponding orbitals f and g.

	f_1	f_2	f_3	f_4
g_1	1.0	0.0	0.0	0.0
g_2	0.0	0.893826	0.0	0.0
g_3	0.0	0.0	0.795833	0.0
g_4	0.0	0.0	0.0	0.795854

Table 5. Occupied corresponding MO of eclipsed carbonless-ethane.

	g_1	g_2	g_3	g_4
1H-1s	0.463480	−0.088375	0.641475	0.0
2H-1s	0.463480	−0.088375	−0.320738	−0.555534
3H-1s	0.463480	−0.088375	−0.320738	0.555534
4H-1s	0.000051	0.471830	0.641475	0.0
6H-1s	0.000051	0.471830	−0.320738	−0.555534
8H-1s	0.000051	0.471830	−0.320738	0.555534

Table 6. Occupied corresponding MO of staggered carbonless-ethane.

	f_1	f_2	f_3	f_4
1H-1s	0.463482	−0.086536	0.651001	0.0
2H-1s	0.463482	−0.086536	−0.325500	−0.563783
3H-1s	0.463482	−0.086536	−0.325500	0.563783
5H-1s	0.000045	0.471491	0.325500	−0.563783
7H-1s	0.000045	0.471491	−0.651001	0.0
9H-1s	0.000045	0.471491	0.325500	0.563783

Table 7. Energy changes in internal rotation.

	E_T	E_{ne}	E_{ee}	E_{el}	E_{NN}	E_{Total}
C_2H_6[b]						
Staggered	79.07193	−267.46447	67.35617	−121.03637	41.93239	−79.10398
Eclipsed	79.08337	−267.49706	67.37488	−121.03881	41.63988	−79.09893
$\Delta(E-S)$	0.01144	−0.03259	0.01871	−0.00244	0.00749	0.00505
kcal/mole	7.18	−20.46	11.74	−1.53	4.70	3.17
H_6						
Staggered	2.63898	−12.92323	3.95845	−6.32580	3.54643	−2.77937
Eclipsed	2.61038	−12.91832	3.95168	−6.35627	3.55392	−2.80235
$\Delta(E-S)$	−0.02860	0.00491	−0.00677	−0.03047	0.00749	−0.02298
kcal/mole	−17.95	3.08	−4.25	−19.13	4.70	−14.43

[a] Energies in atomic units; [b]see Ref. 1; [c]E_T: Kinetic energy; E_{ne}: Nuclear attraction energy; E_{ee}: Electron repulsion energy; E_{el}: Electronic energy; E_{NN}: Nuclear repulsion.

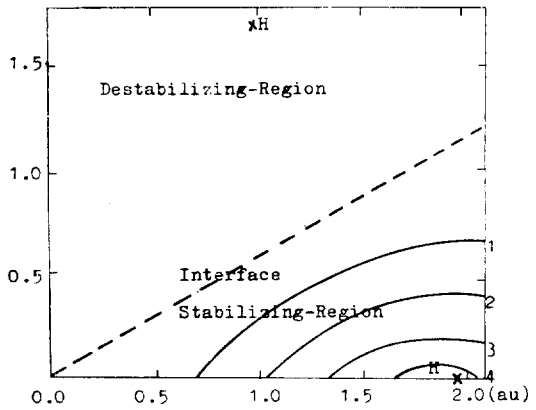

Fig. 3-1. Plot of effective transition density of carbonless ethane at $z=2.5$ au. Contour 1 is at 0.005 au and the contour interval is 0.005 au.

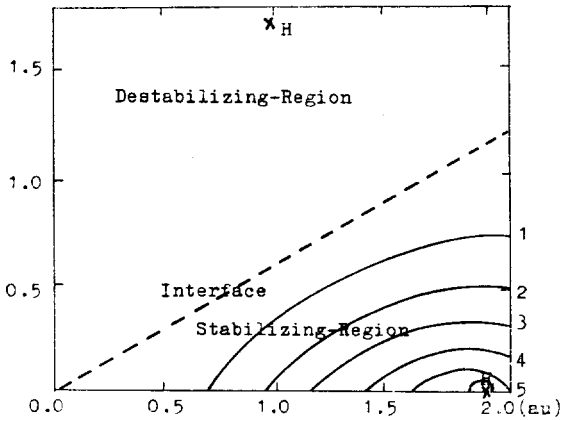

Fig. 3-2. Plot of effective transition density of carbonless ethane at $z=2.157086$ au. Contour 1 is at 0.005 au and the contour interval is 0.005 au.

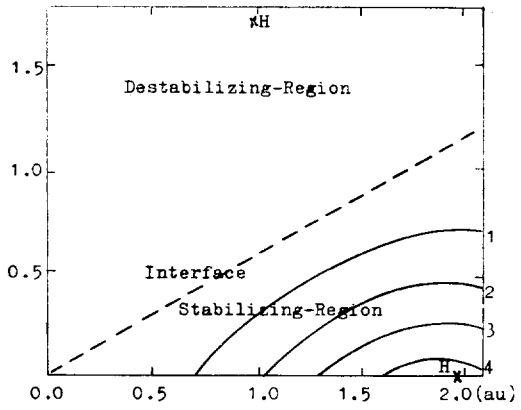

Fig. 3-3. Plot of effective transition density of carbonless ethane at $z=1.8$ au. Contour 1 is at 0.005 au and the contour interval is 0.005 au.

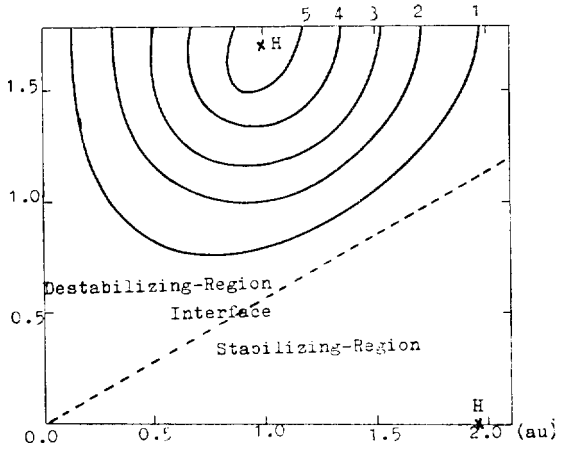

Fig. 4-1. Plot of effective transition density of the real ethane at $z=2.5$ au. Contour 1 is at 0.0001 au and the contour interval is 0.0001 au.

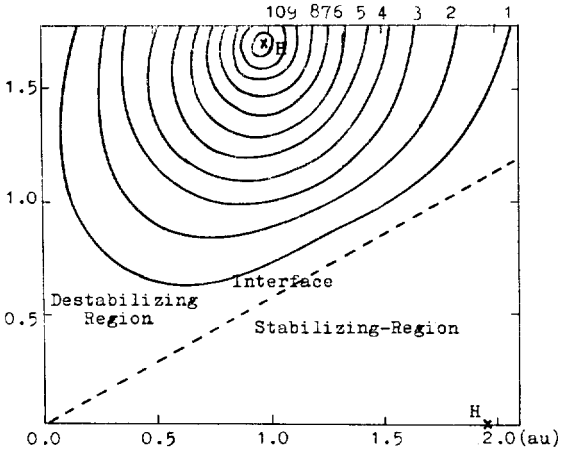

Fig. 4-2. Plot of effective transition density of the real ethane at $z=2.157086$ au, where upper end protons are located. Contour 1 is at 0.0001 au and the contour interval is 0.0001 au.

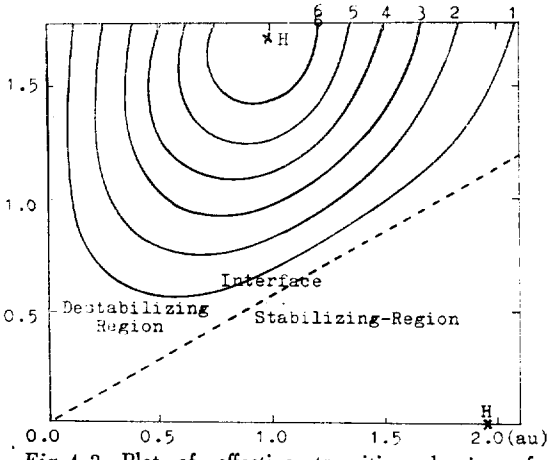

Fig. 4-3. Plot of effective transition density of the real ethane at $z=1.8$ au. Contour 1 is at 0.0001 au and the contour interval is 0.0001 au.

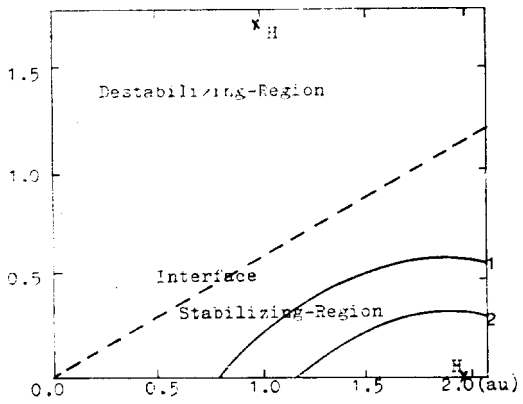

Fig. 3-4. Plot of effective transition density of carbonless ethane at z=1.457935 au. Contour 1 is at 0.005 au and the contour interval is 0.005 au.

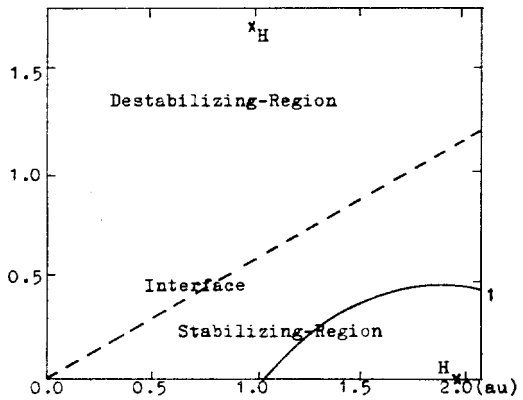

Fig. 3-5. Plot of effective transition density of carbonless ethane at z=1.0 au. Contour 1 is at 0.005 au and the contour interval is 0.005 au.

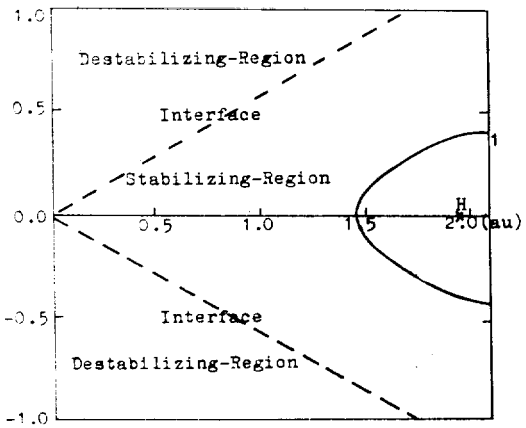

Fig. 3-6. Plot of effective transition density of carbonless ethane at z=0.0 au. Contour 1 is at 0.005 au and the contour interval is 0.005 au.

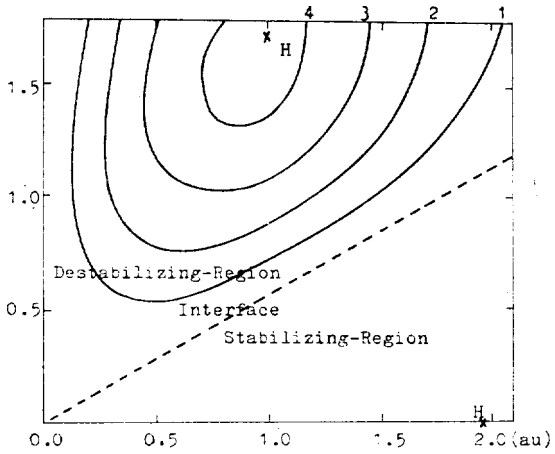

Fig. 4-4. Plot of effective transition density of the real ethane at z=1.457935 au, where upper carbon is located. Contour 1 is at 0.0001 au and the contour interval is 0.0001 au.

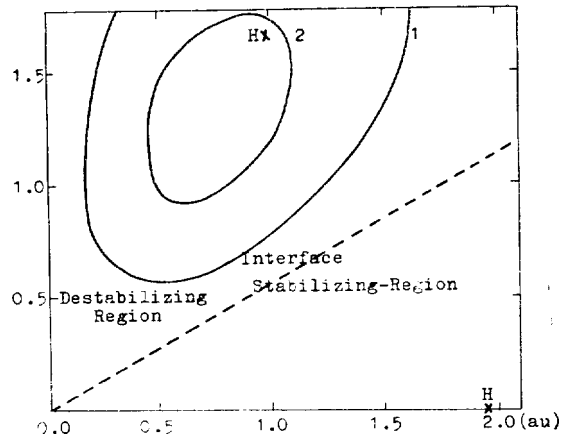

Fig. 4-5. Plot of effective transition density of the real ethane at z=1.0 au. Contour 1 is at 0.0001 au and the contour interval is 0.0001 au.

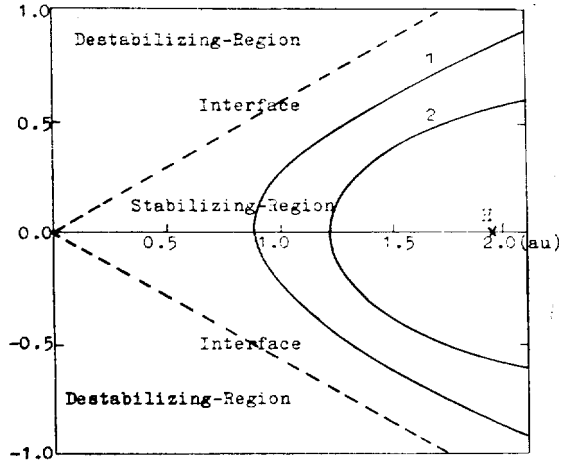

Fig. 4-6. Plot of effective transition density of the real ethane at z=0.0 au. Contour 1 is at 0.001 au and the contour interval is 0.001 au.

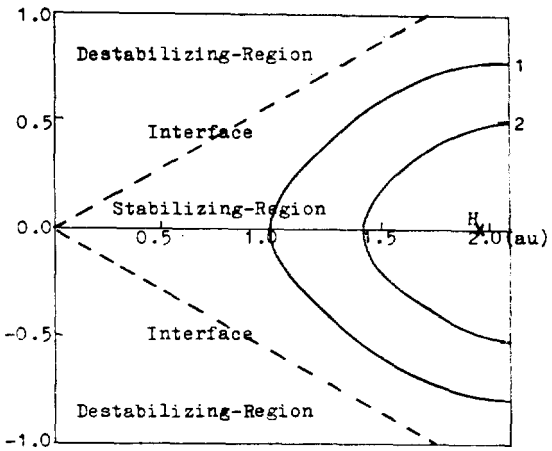

Fig. 3-7. Plot of effective transition density of carbonless ethane at $z=-1.0$ au. Contour 1 is at 0.01 au and the contour interval is 0.01 au.

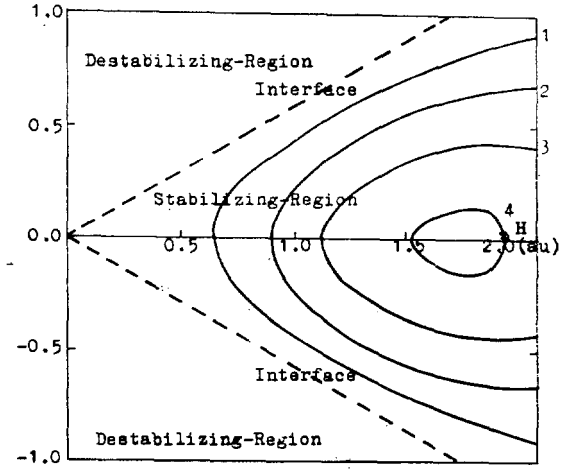

Fig. 4-7. Plot of effective transition density of the real ethane at $z=-1.0$ au. Contour 1 is at 0.01 au and the contour interval is 0.01 au.

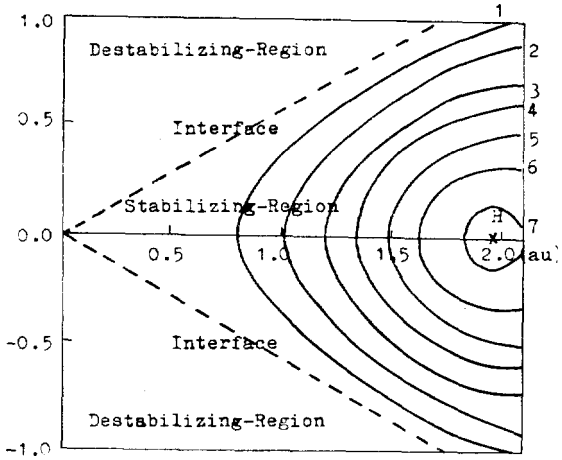

Fig. 3-8. Plot of effective transition density of carbonles ethanes at $z=-1.457935$ au. Contour 1 is at 0.01 au and the contour interval is 0.01 au.

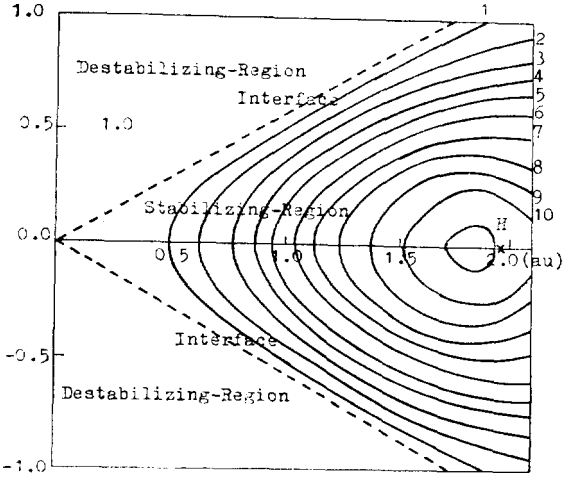

Fig. 4-8. Plot of effective transition density of the real ethane at $z=-1.457935$ au, where lower carbon is located. Contour 1 is at 0.01 au and the contour interval is 0.01 au.

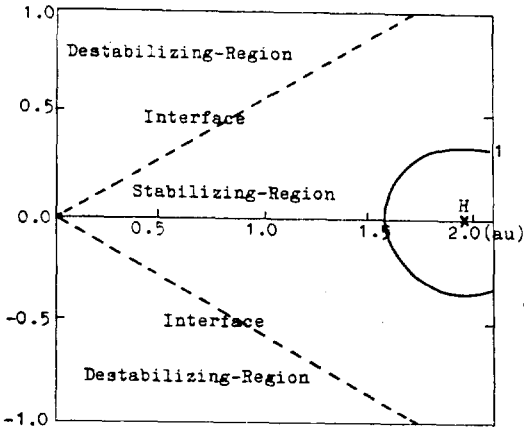

Fig. 3-9. Plot of effective transition density of carbonless ethane at $z=-1.8$ au. Contour 1 is at 0.1 au and the contour interval is 0.1 au.

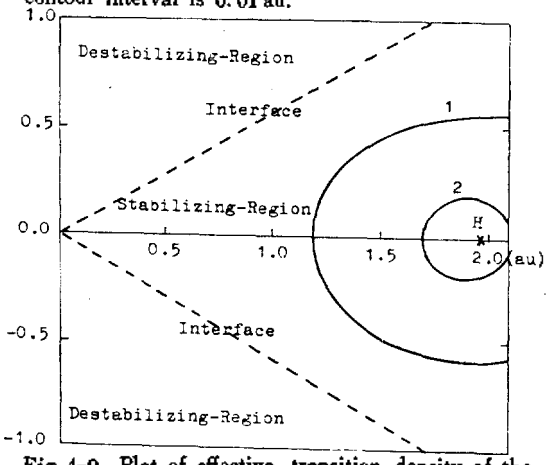

Fig. 4-9. Plot of effective transition density of the real ethane at $z=-1.8$ au, where lower carbon is located. Contour 1 is at 0.1 au and the contour interval is 0.1 au.

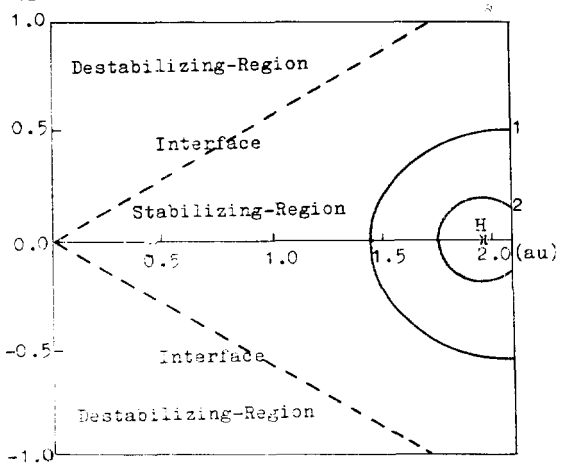

Fig. 3-10. Plot of effective transition density of carbonless ethane at $z=-2.157086$ au. Contour 1 is at 0.1 au and the contour interval is 0.1 au.

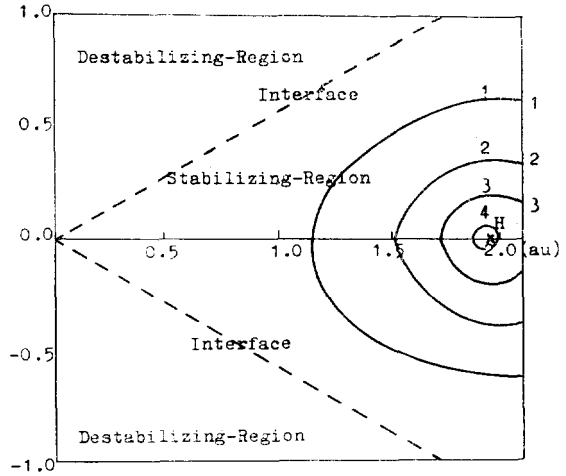

Fig. 4-10. Plot of effective transition density of the real ethane at $z=-2.157086$ au, where lower end protons are located. Contour 1 is at 0.1 au and the contour interval is 0.1 au.

The effective transition density of the carbonless ethane is depicted in *Figs.* 3-1~3-10. For comparison, the effective transition density of the real ethane, obtained in the previous work,[1] is presented in *Figs.* 4-1~4-10.

4. TRANSITION DENSITY ANALYSIS

The IHF perturbation energies of the real ethane and the carbonless ethane is expressed as follows

$$\Delta E^{IHF}_{C_2H_6}(\text{staggered}\rightarrow\text{eclipsed}) = \int \Delta v(1)\rho^{C_2H_6}_{st}(1)d\tau_1 + \Delta E_{NN} \qquad (30)$$

$$\Delta E^{IHF}_{H_6}(\text{staggered}\rightarrow\text{eclipsed}) = \int \Delta v(1)\rho^{H_6}_{st}(1)d\tau_1 + \Delta E_{NN} \qquad (31)$$

It is evident that ΔE_{NN} and $\Delta v(1)$ are common to real ethane and the carbonless ethane.

$$\Delta v(1) = -\left(\sum_p^{ecl.}\frac{1}{r_{p1}}\right) - \left(-\sum_q^{stag.}\frac{1}{r_{q1}}\right) \qquad (32)$$

p: eclipsed protons at the moving end; q: staggered protons at the moving end.

ΔE_{NN} (staggered→eclipsed) is always given exactly if one knows the exact protonic arrangements. Thus the total perturbation energies of the ethane and the carbonless ethane can be compared solely in terms of the electronic perturbation energies, $\Delta E^{C_2H_6}_{el}$ and $\Delta E^{H_6}_{el}$, which in turn could be analyzed through the transition densities, $\rho^{C_2H_6}_{st}(1)$ and $\rho^{H_6}_{st}(1)$. And because of rather large absolute valuse of $\Delta v(1)$ in the vicinity of the moving end protonic sites, the transition density near the sites would be expected to play the crucial role. In the vicinity of the moving end protonic site the effective transition density[1] of the real ethane appears in the Destabilizing-Region.

On the other hand, the effective transition density of the carbonless ethane, in all planes perpendicular to z-axis,[1] is dominated in the Stabilizing-Region. The fact is thus clearly consistent with the large negative value of $\Delta E^{H_6}_{el}$, -19.13 kcal/mole, which can be expected from that the distances between hydrogen atoms in hydrogen molecules of equilibrium conformation. Namely, in the case of the carbonless ethane, the magnitude of electronic energy depression overwhelms the ΔE_{NN}. But on the staggered-to-eclipsed rotation, in the case of ethane, the magnitude of electronic energy depression is not large enough to offset the increased nuclear-nuclear repulsion. And

in the previous work,[1] the transition density of fixed part, $\rho_{tr}^{fix}(1)$, almost completely screen the fixed end proton against the moving end protons and the barrier is originated from the destabilizing effect of $\rho_{tr}^{mov}(1)$. Analysis of transition density (a superposition of the overlap density) contours convinces us that, in the carbonless ethane, the electronic charge in the vicinity of the protonic site becomes concentrated as the staggered-to-eclipsed rotation proceed.

On the other hand, in the real ethane, electronic charge in the vicinity of the protonic site is diluted and is attracted to carbon nucleus as the the barrier traversed. Thus the electronic charge rearrangement which renders the destabilizing effect of $\rho_{tr}^{mov}(1)$, as the barrier is traversed, is caused by the existence of axial atoms (carbon atoms). Due to the axial atoms, the overlap (repulsive) interaction between the opposing C-H bond orbitals becomes a dominant term in the barrier[14]. This is analogous to the Closed-shell repulsion between a pair of helium atoms.

5. CONCLUSION

From *Fig.* 3 and *Fig.* 4, we find that the shift of the effective transition charge density from the stabilizing-region to the destabilizing-region, due to the existence of the axial atoms, causes the decrease of the magnitude of the electronic perturbation energy to such an extent that the change of the nuclear-nuclear repulsion energy becomes the dominant portion of the total perturbation energy.

Thus it is confirmatively found that the barrier of ethane is originated from the dilution of the electronic charge in the vicinity of the protonic sites and from the electronic charge attracting effect of axial carbons as the barrier is traversed.

REFERENCES

1. Hojing Kim, *Proc. Coll. Natur. Sci., SNU*, Vol. 5, No. 1, 69 (1980).
2. R. M. Pitzer and W. N. Lipscomb, *J. Chem. Phys.*, **39**, 1995 (1963).
3. J. L. Dodds and R. McWeeny, *Chem. Phys. Letters*, **13**, 9 (1972).
4. R. McWeeny and B. T. Sutcliffe, "Methods of molecular quantum mechanics," Section 5.4, Academic Press, New York, 1969.
5. R. McWeeny, "Molecular orbitalsin Chemistry, Physics and Biology," Eds., P-O. Löwdin and A. Pullman, P. 305, Academic Press, New York, 1964.
6. J. C. Slater, "Quantum Theory of Molecules and Solids," Vol. 1, McGraw-Hill Book Co. Inc., New York, 1963.)
7. C. C. J. Rootahan, *J. Chem. Phys.*, **19**, 1445 (1951).
8. I. I. Guseinov, *J. Chem. Phys.*, **65**, 4718 (1976).
9. I. I. Guseinov, *J. Phys.*, B3, 1399 (1970).
10. P-O. Löwdin, *J. Chem. Phys.*, **21**, 374 (1953).
11. R. S. Barker, H. Eyring, C. J. Thorn and D. A. Baker, *J. Chem. Phys.*, **22**, 699 (1954).
12. D. B. Cook, "Structures and Approximations for Electrons in Molecules," Ellis Horwood Ltd., Chichester, 1978.
13. I. G. Csizmadia, "Theory and Practice of MO calculations on Organic Molecules," Elsevier Scientific Publishing Co., Amsterdam, 1976.
14. O. J. Sovers, C. W. Kern, P. M. Pitzer and M. Karplus, *J. Chem. Phys.*, **49**, 2592 (1968).
15. R. G. Parr, *J. Chem. Phys.*, **40**, 3726 (1964); H. J. Kim and R. G. Parr, *ibid.*, **41**, 2892 (1964); J. W. Richardson and A. K. Pack, *ibid.*, **41**, 979 (1964).